


Vibration source identification using an energy density method

Chen Mao¹ , Wai On Wong¹ , and Li Cheng¹

Journal of Vibration and Control
2022, Vol. 28(23-24) 3859–3874
© The Author(s) 2021
Article reuse guidelines:
sagepub.com/journals-permissions
DOI: 10.1177/10775463211039903
journals.sagepub.com/home/jvc


Abstract

The localization of shaking forces acting on an operating machine is an important step to identify vibration and noise sources. The forced vibration response of a linearly vibrating structure is assumed to be linear. However, the energy distribution of a linearly vibrating structure contains “coupled terms” in the modal decomposition of the vibration energy density function. These coupled energy terms represent the cross-modal energy density associated with the exciting force of a dynamic structure under forced vibration. In this research, it is proved analytically that the high-order cross-modal energy densities of a linear dynamic structure are highly correlated to the location of the external exciting force. Using this finding, a new force localization index based on the high-order cross-modal energy densities of a dynamic structure is proposed and tested. Numerical tests on uniform and step beam structures under force excitation with different frequencies and locations have been carried out to test the effectiveness of the proposed force localization method. It is found that the proposed force localization method works well on vibrating beam structures. Experiments are carried out to verify the proposed force localization method.

Keywords

Vibration source identification, force localization, energy density, vibration energy

1. Introduction

The localization of dynamic forces acting on a structure is important in locating the vibration and noise sources. In many practical cases, it may not be possible to measure the dynamic force directly and detection of unknown forces from vibration measurements at accessible locations is required. A large number of studies have been conducted about indirect determination of the dynamic loadings by calculating the forces through the measured frequency response function (FRF) matrix and structural operational response with a mathematical model of the structure as an inverse problem (Ma et al., 2003; Thite and Thompson, 2003; Djamaa et al., 2007; Janssens et al., 2011; Lage et al., 2013). In practice, the measurement of the FRF of a dynamic system takes a long time, and in many cases, the ill-posedness of the force identification problem results in large estimation errors. New force identification methods were developed in order to avoid measuring the FRF matrix. Force analysis technique (FAT) (Pezerat and Guyader, 2000a and 2000b; Leclere and Pezerat, 2012) is based on the numerical discretization of the equation of motion of the structure. Due to the difficulty in formulating the equations of motion of the dynamic structures in practical applications, some researchers investigate the function expansion method (Jiang et al., 2019; Lee et al., 2006; Li et al., 2015; Qiao et al., 2015, 2016). The function expansion method

employs appropriate basis functions to approximate the desired unknown force. The coefficients of basis functions are solved instead of the original force and the number of unknowns is significantly reduced. The exciting force to a dynamic structure can also be identified as the energy source of the structural intensity or power flow in the structure (Wang et al., 2006; Samet et al., 2017). The force identification in all the abovementioned methods is considered as a classical inverse problem, in which the measured data and the assumed mathematical models of mechanical structures are used to determine the applied force. However, the analysis results of the abovementioned methods are often contaminated by the noise generated during the derivation of the high-order derivatives of the measured vibration signal and the local change of the structure in mass and stiffness (Pezerat and Guyader 2000a; Lee et al., 2006; Wang et al., 2006; Xu et al. 2011).

¹Department of Mechanical Engineering, Hong Kong Polytechnic University, Kowloon, China

Received: 10 March 2021; accepted: 27 July 2021

Corresponding author:

Wai On Wong, Department of Mechanical Engineering, Hong Kong Polytechnic University, Hong Kong Polytechnic University, Hung Hom, Hong Kong SAR China, Kowloon 852, China.
Email: mmwong@polyu.edu.hk

Based on the review of force identification methods, there are two major difficulties found in the recently developed methods: (1) the contamination of force identification index caused by non-uniform geometry or properties of the structure and (2) amplification of noise in the generation of high-order derivatives of the vibration signal.

In this article, we propose an alternative approach for the identification of dynamic loads in structures based on concepts different from those presented previously. There have been some studies on the relationship between the modal vibration energy (Wong et al., 2009; Wang et al., 2009) and structural damages of structures. This article presents an analysis of the effect on the redistribution of the cross-modal energy density of a continuous structure by the exciting force. A force localization method is established based on the determination of the cross-modal energy density function of the vibrating structure as described in the following section. A force localization index is constructed by relating the change of vibration energy distribution of the structure caused by the exciting force. The proposed method is proved analytically to work on non-uniform beam structures and it does not require the determination of high-order derivative of the vibration signal.

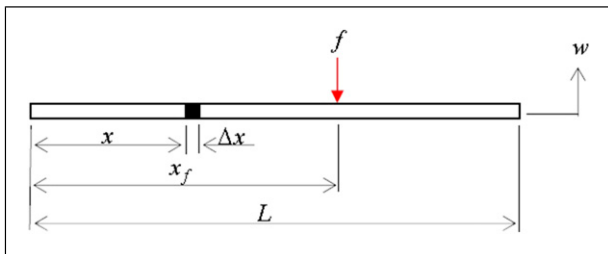


Figure 1. Illustration of the transverse vibration w of a beam excited by a dynamic point force f at $x = x_f$.

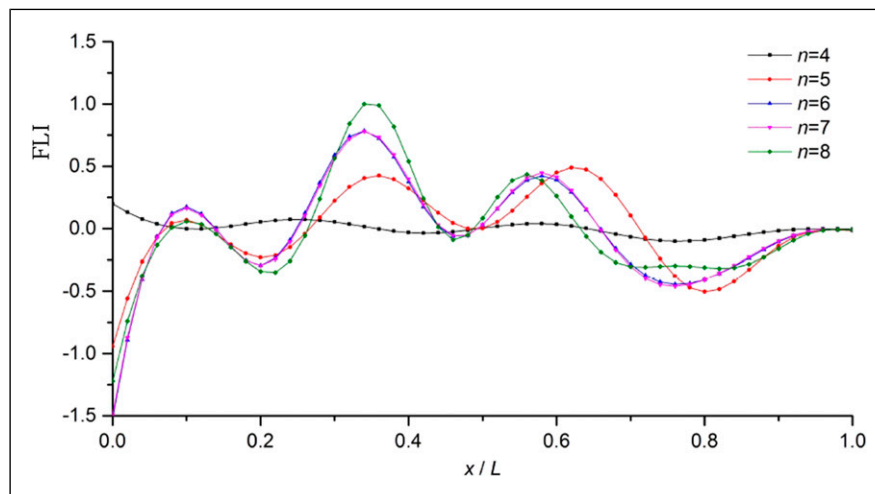


Figure 2. Force localization index (FLI) of a beam with fixed-free boundary conditions ($x_f = 0.35L$).

Both simulation and experimental tests are carried out to provide validations of the proposed force localization method.

2. Theory

Considering the forced vibration of a uniform Euler beam as illustrated in Figure 1, the equation of motion of the beam may be written as (Meirovitch, 2001)

$$m(x) \frac{\partial^2 w(x,t)}{\partial t^2} + \frac{\partial^2}{\partial x^2} \left[YI(x) \frac{\partial^2 w(x,t)}{\partial x^2} \right] = F \delta(x - x_f) \sin(\omega t), \quad 0 < x < L \quad (1)$$

where $w(x,t)$ is the transverse displacement, $m(x)$ is the mass per unit length, and L is the length of the beam. $YI(x)$ is the flexural rigidity, in which Y is the Young's modulus and $I(x)$ is the second moment of cross-sectional area of the beam. δ is the Kronecker delta function. $f = F \sin \omega t$ is the exciting harmonic force of frequency ω acting at point $x = x_f$.

The vibration energy of the beam may be written as

$$E(t) = T(t) + V(t) = \frac{1}{2} \int_0^L m \left[\frac{\partial w(x,t)}{\partial t} \right]^2 dx + \frac{1}{2} \int_0^L YI \left[\frac{\partial^2 w(x,t)}{\partial x^2} \right]^2 dx \quad (2)$$

where $E(t)$ is the total vibration energy of the beam composed of the kinetic energy $T(t)$ and strain energy $V(t)$.

The vibration energy of an infinitesimal element of length Δx , as shown in Figure 1, may be written as

$$\Delta E(x,t) = \Delta T(x,t) + \Delta V(x,t) = \frac{1}{2} m(\Delta x) \dot{w}(x,t)^2 + \frac{1}{2} YI \left[\frac{\partial^2 w(x,t)}{\partial x^2} \right]^2 (\Delta x) \quad (3)$$

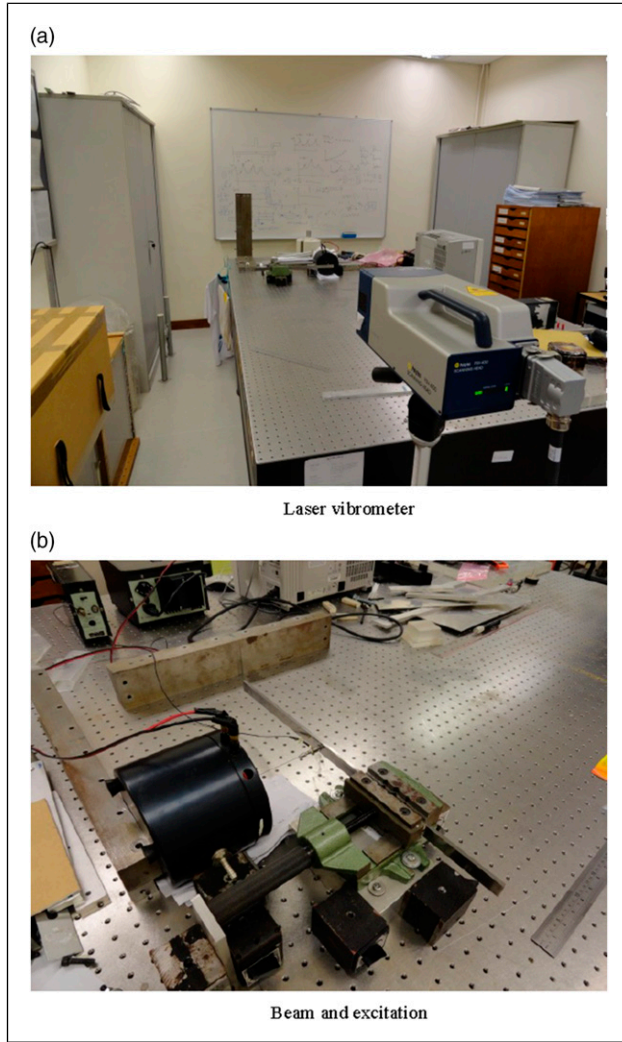


Figure 3. Setup of the experiments.

where $\dot{w}(x,t)$ represents $\partial w(x,t)/\partial t$. The energy density function $e(x,t)$ is defined as (Wong et al., 2009)

$$\begin{aligned} e(x,t) &= \lim_{\Delta x \rightarrow 0} \frac{\Delta E(x,t)}{\Delta x} = \frac{\partial E}{\partial x} = \frac{\partial T}{\partial x} + \frac{\partial V}{\partial x} \\ &= \frac{1}{2} m \dot{w}(x,t)^2 + \frac{1}{2} YI \left[\frac{\partial^2 w(x,t)}{\partial x^2} \right]^2 \end{aligned} \quad (4)$$

2.1. Decomposition of the vibration energy

The solution of equation (1) may be written as

$$w(x,t) = \sum_{i=1}^{\infty} \eta_i \varphi_i(x) \sin(\omega t) \quad (5)$$

where $\varphi_i(x)$ is the i^{th} vibration mode shape of the beam and η_i is the i^{th} modal ratio coefficient written as

$$\eta_i = \frac{\int_0^L \varphi_i(x) F \delta(x - x_f) dx}{\omega_i^2 - \omega^2} = \frac{F \varphi_i(x_f)}{\omega_i^2 - \omega^2} \quad (6)$$

where ω_i is the i^{th} natural frequency of the beam.

Substituting equation (5) into equation (4), $e(x,t)$ can be rewritten as

$$\begin{aligned} e(x,t) &= \frac{1}{2} m \omega^2 \left(\sum_{i=1}^{\infty} \eta_i \varphi_i(x) \right)^2 \cos^2 t \\ &\quad + \frac{1}{2} YI \left(\sum_{i=1}^{\infty} \eta_i \frac{\partial^2 \varphi_i(x)}{\partial x^2} \right)^2 \sin^2 t \\ &= \frac{1}{2} \left(\frac{1}{2} m \omega^2 \left(\sum_{i=1}^{\infty} \eta_i \varphi_i(x) \right)^2 \right. \\ &\quad \left. + \frac{1}{2} YI \left(\sum_{i=1}^{\infty} \eta_i \frac{\partial^2 \varphi_i(x)}{\partial x^2} \right)^2 \right) \\ &\quad + \frac{1}{2} \left(\frac{1}{2} m \omega^2 \left(\sum_{i=1}^{\infty} \eta_i \varphi_i(x) \right)^2 \right. \\ &\quad \left. - \frac{1}{2} YI \left(\sum_{i=1}^{\infty} \eta_i \frac{\partial^2 \varphi_i(x)}{\partial x^2} \right)^2 \right) \cos(2\omega t) \\ &= E(x) + L(x) \cos(2\omega t) \end{aligned} \quad (7)$$

where

$$\begin{aligned} E(x) &= \frac{1}{2} \left(\frac{1}{2} m(x) \omega^2 \left(\sum_{i=1}^{\infty} \eta_i \varphi_i(x) \right)^2 \right. \\ &\quad \left. + \frac{1}{2} YI(x) \left(\sum_{i=1}^{\infty} \eta_i \frac{\partial^2 \varphi_i(x)}{\partial x^2} \right)^2 \right) \end{aligned} \quad (8a)$$

$$\begin{aligned} L(x) &= \frac{1}{2} \left(\frac{1}{2} m(x) \omega^2 \left(\sum_{i=1}^{\infty} \eta_i \varphi_i(x) \right)^2 \right. \\ &\quad \left. - \frac{1}{2} YI(x) \left(\sum_{i=1}^{\infty} \eta_i \frac{\partial^2 \varphi_i(x)}{\partial x^2} \right)^2 \right). \end{aligned} \quad (8b)$$

The static or time-unvarying component, $E(x)$, is the mean total energy density, whose integration along the beam gives the total energy of the beam. The amplitude of the dynamic or time-varying component in equation (7), $L(x)$, on the other hand, represents the mean Lagrangian energy density (Wong et al., 2009; Wang et al., 2009). The dynamic component, $L(x) \cos(2\omega t)$, implies that there exists instantaneous energy exchange between adjacent beam elements at double frequency of the vibration motion of the beam.

The static or mean energy density is considered in the following analysis. It is rewritten as

$$\begin{aligned}
 E(x) &= \sum_{j=1}^{\infty} \sum_{k=1}^{\infty} \frac{1}{2} \left(\frac{1}{2} m \omega_f^2 \varphi_j(x) \varphi_k(x) \right. \\
 &\quad \left. + \frac{1}{2} YI \frac{d^2(\varphi_j(x))}{dx^2} \frac{d^2(\varphi_k(x))}{dx^2} \right) \eta_j \eta_k \quad (9) \\
 &= \sum_{j=1}^{\infty} \sum_{k=1}^{\infty} E_{jk}(x) \eta_j \eta_k
 \end{aligned}$$

where

$$\begin{aligned}
 E_{jk}(x) &= \frac{1}{2} \left(\frac{1}{2} m \omega_f^2 \varphi_j(x) \varphi_k(x) \right. \\
 &\quad \left. + \frac{1}{2} YI \frac{d^2(\varphi_j(x))}{dx^2} \frac{d^2(\varphi_k(x))}{dx^2} \right) \quad (10)
 \end{aligned}$$

Using equation (9), the mean energy density $E(x)$ can be written in matrix form as

$$\begin{aligned}
 E(x) &= [\eta_1, \eta_2, \dots] \begin{bmatrix} E_{11}(x) & \dots & E_{1k}(x) & \dots \\ \vdots & \ddots & \vdots & \vdots \\ E_{j1}(x) & \dots & E_{jk}(x) & \dots \\ \vdots & \vdots & \vdots & \ddots \end{bmatrix} \begin{bmatrix} \eta_1 \\ \eta_2 \\ \vdots \\ \vdots \\ \vdots \end{bmatrix} \\
 &= \sum_{i=1}^{\infty} E_{ii}(x) \eta_i^2 + \sum_{\substack{j=1 \\ j \neq k}}^{\infty} \sum_{\substack{k=1 \\ k \neq j}}^{\infty} E_{jk}(x) \eta_j \eta_k \\
 &= E_{\text{dia}}(x) + E_{\text{cross}}(x) \quad (11)
 \end{aligned}$$

where $E_{\text{dia}}(x) = \sum_{i=1}^{\infty} E_{ii}(x) \eta_i^2$ and $E_{\text{cross}}(x) = \sum_{\substack{j=1 \\ j \neq k}}^{\infty} \sum_{\substack{k=1 \\ k \neq j}}^{\infty} E_{jk}(x) \eta_j \eta_k$

The amplification coefficient is defined as

$$\Gamma_{jk} = \eta_j \eta_k = \frac{\varphi_j(x_f) \varphi_k(x_f) F^2}{(\omega_j^2 - \omega^2)(\omega_k^2 - \omega^2)} \quad (12)$$

2.2. Interpretation of the vibration energy decomposition

Equation (11) shows that the mean energy density is composed of $E_{\text{dia}}(x)$ and $E_{\text{cross}}(x)$. $E_{ii}(x)$ of $E_{\text{dia}}(x)$ represents the i^{th} modal energy density distribution in the beam caused by the exciting harmonic force, and $\int_0^L E_{ii}(x) dx$ represents the i^{th} modal energy stored in the beam. The integration of the mean energy density along the beam can be written as

$$\begin{aligned}
 \int_0^L E(x) dx &= \int_0^L E_{\text{dia}}(x) dx + \int_0^L E_{\text{cross}}(x) dx \\
 &= \int_0^L \sum_{i=1}^{\infty} E_{ii}(x) \Gamma_{ii} dx + \int_0^L \sum_{\substack{j=1 \\ j \neq k}}^{\infty} \sum_{\substack{k=1 \\ k \neq j}}^{\infty} E_{jk}(x) \Gamma_{jk} dx \\
 &= \sum_{i=1}^{\infty} \Gamma_{ii} \int_0^L E_{ii}(x) dx + \sum_{\substack{j=1 \\ j \neq k}}^{\infty} \sum_{\substack{k=1 \\ k \neq j}}^{\infty} \Gamma_{jk} \int_0^L E_{jk}(x) dx \quad (13)
 \end{aligned}$$

According to equation (9), $E_{ii}(x) > 0$. We may write

$$\int_0^L E_{ii}(x) dx > 0, i = 1 \dots n \dots \quad (14)$$

On the other hand, the cross-modal energy density element $E_{jk}(x)$, $j \neq k$ can be positive or negative. The three classical boundary conditions, including pinned, fixed, and free end, render the system self-adjoint (Tse et al., 1978), and therefore, if the mode shapes are mass-normalized, the alternative companion orthonormality relations can be written as (Meirovitch, 2001)

$$\int_0^L YI(x) \frac{d^2 \varphi_j(x)}{dx^2} \frac{d^2 \varphi_k(x)}{dx^2} dx = \delta_{jk}, j, k = 1, \dots, n, \dots \quad (15)$$

where $\delta_{jk} = 1$ if $j = k$ and $\delta_{jk} = 0$ if $j \neq k$.

The orthonormality relation is

$$\int_0^L m \varphi_j(x) \varphi_k(x) dx = \delta_{jk}, j, k = 1, \dots, n, \dots \quad (16)$$

Using equations (15) and (16), the integration of cross-modal energy density element over the beam is

$$\int_0^L E_{jk}(x) dx = 0, j \neq k; j, k = 1, \dots, n, \dots \quad (17)$$

Therefore, $E_{\text{cross}}(x) = \sum_{\substack{j=1 \\ j \neq k}}^{\infty} \sum_{\substack{k=1 \\ k \neq j}}^{\infty} E_{jk}(x) \cdot \eta_j \eta_k$

may be considered as the redistribution of the energy density within the structure. According to equation (11), this shift is found to be related to Γ_{jk} , and from equation (12), Γ_{jk} is related to the location and driving frequency of exciting force. Therefore, $E_{\text{cross}}(x)$ may be considered as the redistribution of energy density caused by the exciting force.

2.3. Force localization index

The cross-modal energy density of the beam may be written as

$$\Gamma_{jk} E_{jk}(x) = \frac{F^2 \varphi_j(x_f) \varphi_k(x_f)}{2(\omega_j^2 - \omega^2)(\omega_k^2 - \omega^2)} \left[\frac{1}{2} m(x) \omega^2 \varphi_j(x) \varphi_k(x) + \frac{1}{2} YI(x) \varphi_j''(x) \varphi_k''(x) \right], j \neq k \tag{18}$$

where

$$\varphi_j''(x) = d^2(\varphi_j(x))/dx^2 \quad \text{and} \quad \varphi_k''(x) = d^2(\varphi_k(x))/dx^2.$$

It can be seen that the value of $\Gamma_{jk} E_{jk}(x)$ in equation (18) is decided by the location x_f and the order of modes j and k . This value varies with the order of modes j and k , and thus may be positive or negative. However, at the location of exciting force x_f , $\Gamma_{jk} E_{jk}(x)$ can be written as

$$\Gamma_{jk} E_{jk}(x_f) = \frac{F^2}{4(\omega_j^2 - \omega^2)(\omega_k^2 - \omega^2)} \times [m(x) \omega^2 \varphi_j(x_f)^2 \varphi_k(x_f)^2 + YI(x) \varphi_j(x_f) \varphi_k(x_f) \varphi_j''(x_f) \varphi_k''(x_f)], j \neq k \tag{19}$$

If only the high-order modes are considered, where $\omega_j > \omega$ and $\omega_k > \omega$, the term $F^2/4(\omega_j^2 - \omega^2)(\omega_k^2 - \omega^2)$ in equation (19) must be positive. The term $m(x) \omega^2 \varphi_j(x_f)^2 \varphi_k(x_f)^2$ in equation (19) is also positive. As shown in the Appendix A, the term $YI(x) \varphi_j(x_f) \varphi_k(x_f) \varphi_j''(x_f) \varphi_k''(x_f)$ in equation (19) can be proved to be positive for $0 < x_f < L$ of a pinned-pinned beam and it is positive for a beam with pinned-fixed/free or fixed/free-fixed/free boundary conditions if x_f is not too close to the fixed/free end of the beam. Quantification of the required distance from the end of the beam is derived and shown in Appendix B.

In view of the abovementioned reasons, the cross-modal energy density $\Gamma_{jk} E_{jk}(x_f)$ is positive at any high-order mode with $\omega_j > \omega$ and $\omega_k > \omega$. Therefore, the sum of high-order terms of $\Gamma_{jk} E_{jk}(x_f)$ with $\omega_j > \omega$ and $\omega_k > \omega$ would show an accumulation phenomenon at the location of the exciting force as illustrated in Figure 2.

Since the accumulation phenomenon of high-order cross-modal energy density is directly related to the force location, a force localization index (FLI) is defined as

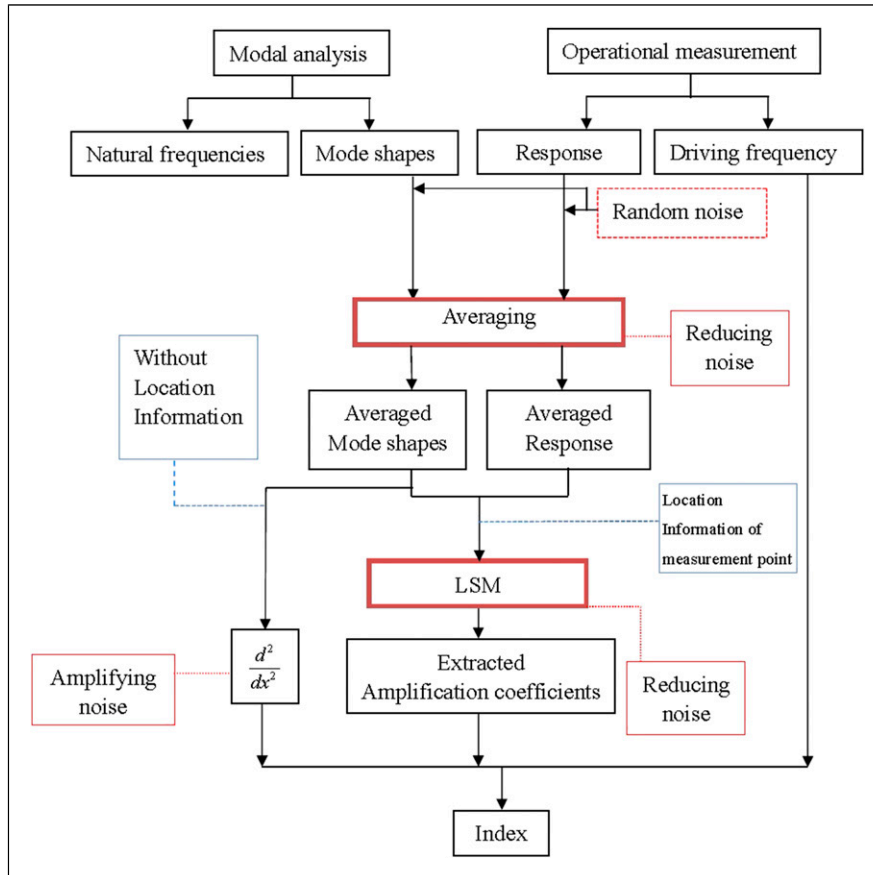


Figure 4. Outline of the experiment procedure.

$$\begin{aligned}
 \text{FLI} &= \sum_{j \neq k}^n \alpha \sum_{k \neq j}^n = \alpha \eta_j \eta_k E_{jk}(x) \\
 &= \sum_{j \neq k}^n \alpha \sum_{k \neq j}^n = \alpha \Gamma_{jk} E_{jk}(x); \quad \omega_j > \omega \quad \text{and} \quad \omega_k > \omega.
 \end{aligned}
 \tag{20}$$

where α and n are selected integers to control the number of high-order mode in the calculation of the FLI. The proposed FLI is tested with a uniform beam numerically and experimentally for force localization and the test results are shown in the following section.

3. Simulation and experiment

A mild steel beam structure was used in both simulation and experiment. The beam had a rectangular cross section under fixed-free boundary condition. The length of it was $L = 0.3$ m. The height and the width of the beam were $h = 0.0047$ m and $b = 0.0191$ m, respectively. The density and Young’s modulus were $\rho = 7740$ kg/m³ and 204 GPa, respectively.

3.1. Simulation

The force localization index (FLI) was calculated according to equation (20) using MATLAB and plotted in Figure 2 for illustration of the proposed force localization method. The exciting force was assumed to be applied at $x_f = 0.35L$ with driving frequency $\omega_f = 300\pi$ rad/s, and the parameter α in equation (20) was chosen to be 1. The accumulation phenomenon of the FLI was noted at the location of exciting force as the parameter n in equation (20) increased from 4 to 8.

3.2. Experiment

In practice, the amplification coefficient Γ_{jk} in equation (20) is unknown and it has to be obtained from the measured operational response of the structure. Least squares method (LSM) (Liu and Shepard, 2005) was applied in the experiments in order to reduce the noise influence in the measurements. The procedure of extracting the amplification coefficient as a typical inverse problem is shown in the following section.

3.2.1. Procedure of experiment. In the experiment, the tested cantilever beam was excited by a concentrated force applied by a shaker (B&K Type 4809), which was powered by power amplifier (B&K Type 2706). The exciting force was measured by using a force transducer (B&K Type 8203). The modal parameters and operational response were measured by using a laser vibrometer (Polytec PSV-400). The whole experiment setup is illustrated in Figure 3.

The outline of experiment is illustrated by Figure 4. It could be found that the random noise in the measurement may influence both the amplification coefficient and modal energy density in equation (20). Since the force location information

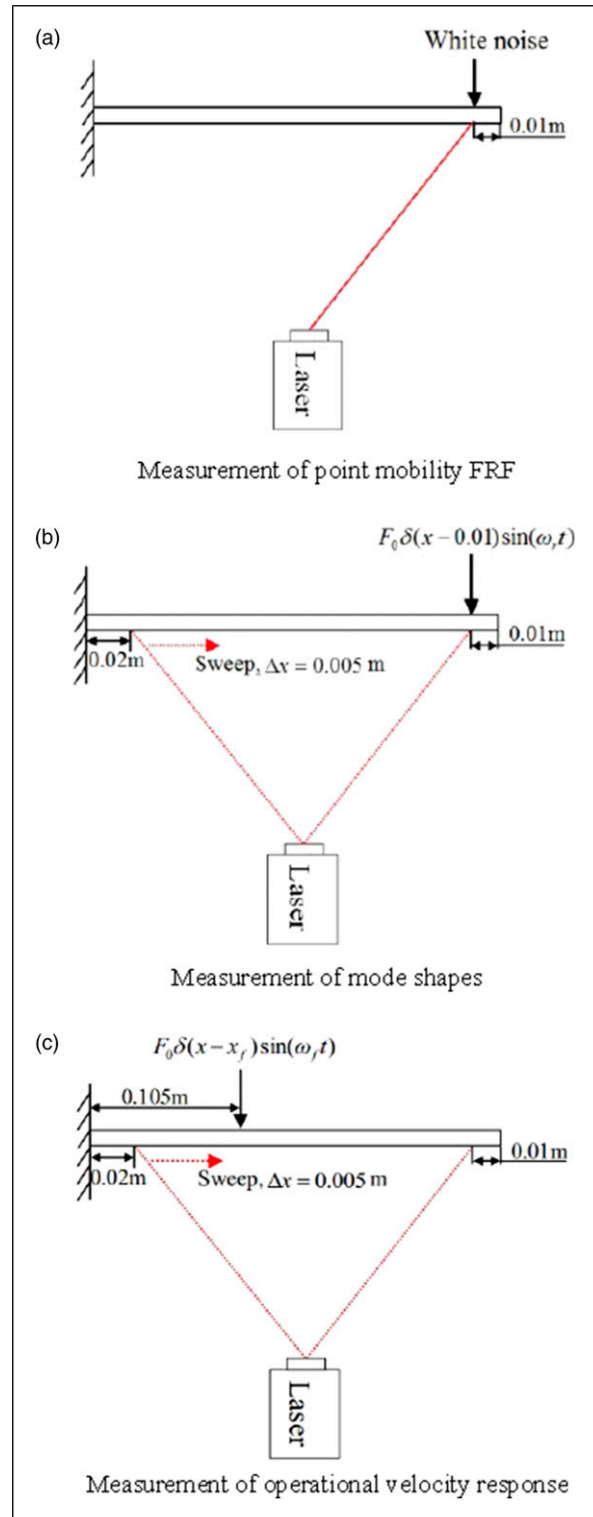


Figure 5. Measurement procedures of the experimental tests.

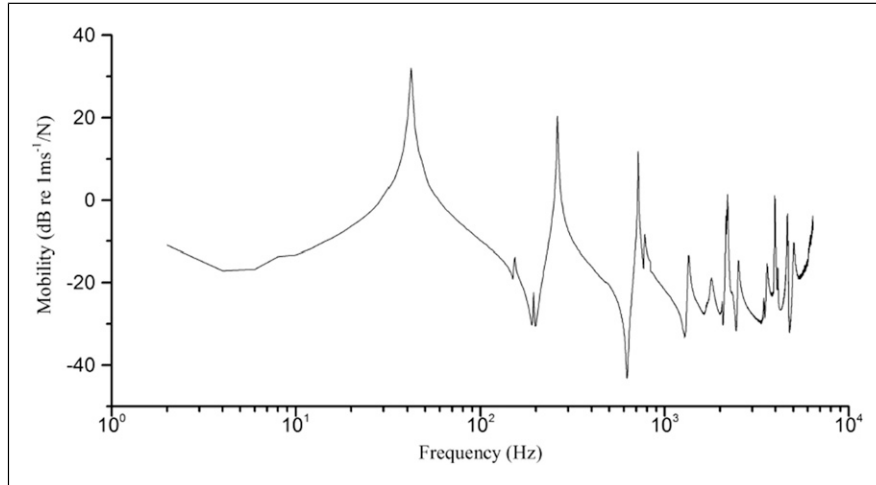


Figure 6. Measured point mobility FRF.

was contained in the amplification coefficient, the amplification of noise caused by high-order derivative in modal energy density element had limited effect on the proposed FLI.

The natural frequencies of the beam were extracted from the standard modal testing software after curve fitting of the FRF. The mode shapes of the beam were measured by exciting the fixed-free beam at the free end with corresponding natural frequencies. The velocity response of the beam was measured with the beam excited by the shaker at the operational frequency.

The measurement procedure was illustrated in Figure 5. As shown in Figure 5(a), the excitation and measurement points for measuring point mobility FRF were chosen at the location 0.01 m away from the free end. White noise was applied to obtain the result in a broad-frequency band. In Figure 5(b), the beam was excited by the exciting force under the natural frequency ω_f at the same location to get the corresponding mode shape. The laser vibrometer swept from the point 0.02 m away from fixed end to the point 0.01 m away from free end, and the interval between two measured points is 0.005 m. In Figure 5(c), the setting of the sweeping range was the same as that in Figure 5(b), and the exciting force was applied at the operational location $x_f = 0.35L$ with the driving frequency $\omega_f = 300\pi$ rad/s. Only the first seven mode shapes were measured as the measurements of the higher mode shapes are less accurate and in practice only limited mode shapes are available.

In the experiment, the point mobility FRF was approximated by using the H2 frequency response estimator for single input single output (SISO) systems with 500-times the complex average. The modal shapes and operational displacement response were measured with 500-times magnitude averaging. The operational response and mode shapes were measured at a finite number of discrete points. Using

equation (5), the measured displacement values of the beam may be put into the following equation

$$w(x) = [W_1(x) \ W_2(x) \ \cdots \ W_n(x)] \cdot \eta = \mathbf{W} \cdot \eta \quad (21)$$

where $w(x)$ and $W_i(x)$ were both $m \times 1$ vectors, and η was a $n \times 1$ vector. m was the number of measured points and n was the number of included modes. The truncation error was neglected.

In order to minimize the difference between the extracted coefficients and the theoretical ones, the LSM was applied to obtain the solution. The modal ratio coefficients can be estimated as

$$\eta = (\mathbf{W}^T \mathbf{W})^{-1} \mathbf{W}^T w(x) \quad (22)$$

The amplification coefficients Γ_{jk} could then be calculated according to equation (12). The cross-modal energy density function $E_{jk}(x)$ could be calculated using the measured mode shapes of the beam. The force localization index (FLI) could then be calculated according to equation (20).

3.2.2. Results of experiment. The measured point mobility FRF and the extracted mode shapes are shown in Figures 6 and 7, respectively. The modal ratio coefficients, which were directly related to the amplification coefficients, were extracted by LSM on the basis of the measured data. The coefficients were normalized to compare with the theoretical ones and listed in Table 1. The coefficient of order 7 as shown in Table 1 was practically zero, so it means orders 7 or higher had negligible effect to the force localization index in this case. The proposed force localization index was calculated according to equations (19) and (20), and the result was shown in Figure 8, where α was 1.

As predicted in theory and illustrated in the simulation, it could be found that the accumulation phenomenon occurred

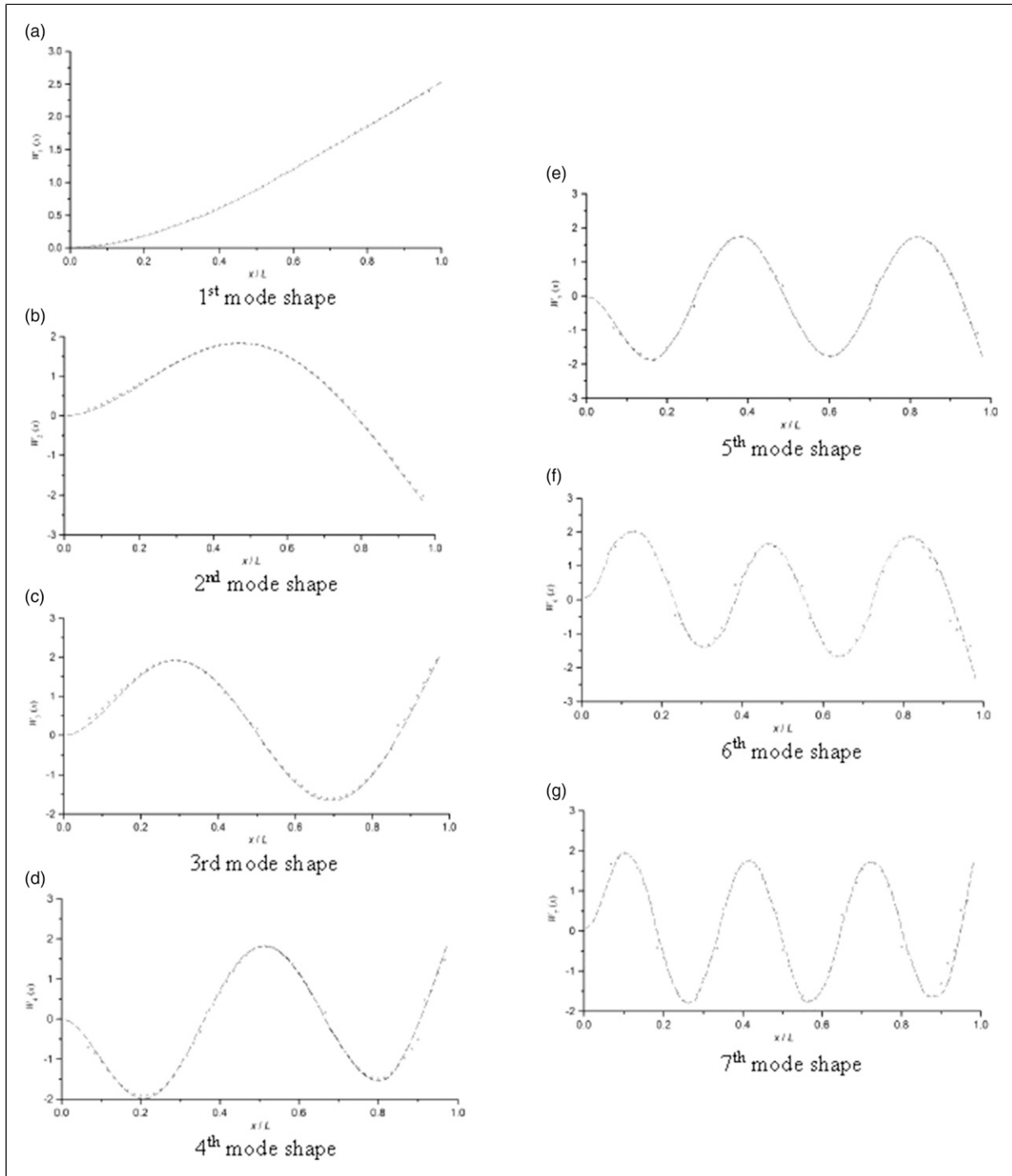


Figure 7. Measured mode shapes of the beam in Figure 5.

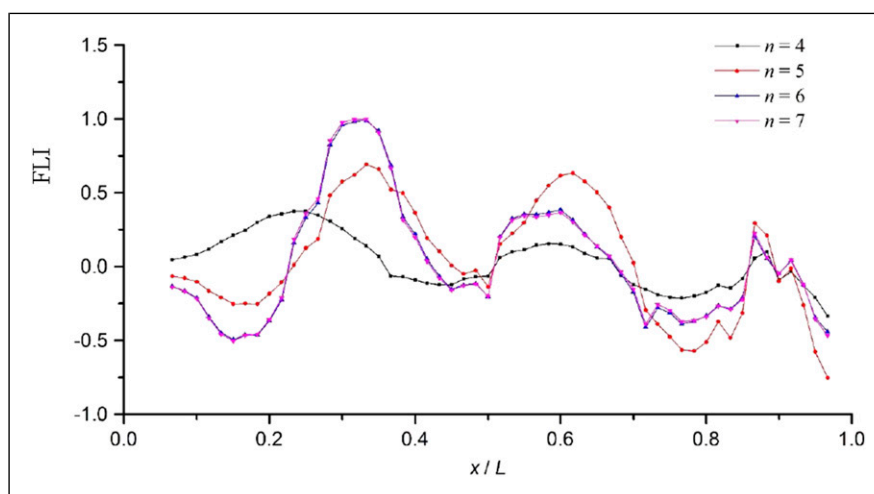
at the location of exciting force as shown in Figure 8. Points at the peaks and troughs of the curve with $n = 7$ in Figure 2 are added and marked with \times for comparison. The locations, x/L , of those points with $n = 7$ in Figure 2 match with the location of the peaks and troughs of the curve with $n = 7$ in Figure 8. The experimental result matched with the

simulation result in Figure 2. The influence of noise in experiment on the extraction of amplification coefficients shown in Table 1 was limited. The proposed force localization method was validated by experiment.

The proposed approach of force localization was extended to test on a step beam or shaft which is more

Table 1. Theoretical and experimental modal ratio coefficients.

Order	η_r (experimental)	η_r (theoretical)	Euclidean distance
1	1	1	0.0303
2	-1.3849	-1.3765	
3	-0.1532	-0.1414	
4	0.0072	-0.0034	
5	-0.0130	0.0113	
6	0.0076	0.0051	
7	5.0409×10^{-4}	-2.4328×10^{-4}	

**Figure 8.** Force localization index derived from experiment ($x_f = 0.35L$). Points at the peaks and troughs of the curve with $n = 7$ in Figure 2 are added and marked with \times for comparison.

common in practice. The analytical eigenvalues and eigenfunctions of the step beam were derived and then the FLI of the step beam was calculated according to equation (20). The derivations and numerical experiment on the step beam were presented in Appendix B.

4. Conclusion

A force localization method was established theoretically based on the accumulation phenomenon of the high-order cross-modal energy density at the excitation location. The redistribution of cross-modal energy density of a uniform or step beam under forced vibration was derived analytically as a function of the location of the exciting force. It was analytically proved that the cross-modal energy density of the beam with any classical boundary condition including pinned, free, and fixed ends would accumulate at the location of the exciting force provided that the force was not too close to the boundary in case of a free or fixed end. Based on this accumulation phenomenon, selected high-order cross-modal energy density was used as an index to identify the location of the exciting force. The proposed method

was validated by both numerical and experimental tests on a cantilever beam.

Acknowledgments

The authors thank The Hong Kong Polytechnic University for the funding support in this research project.

Declaration of conflicting interests

The author(s) declared no potential conflicts of interest with respect to the research, authorship, and/or publication of this article.

Funding

The author(s) disclosed receipt of the following financial support for the research, authorship, and/or publication of this article: The Hong Kong Polytechnic University, (Grant / Award Number: '11901157R')

ORCID iDs

Chen Mao  <https://orcid.org/0000-0002-3399-6436>

Wai On Wong  <https://orcid.org/0000-0003-3448-8836>

References

- Djamaa MC, Ouelaa N, Pezerat C, et al. (2007) Reconstruction of a distributed force applied on a thin cylindrical shell by an inverse method and spatial filtering. *Journal of Sound and Vibration* 301: 560–575.
- Janssens K, Gajdatsy P, Gielen L, et al. (2011) OPAX: a new transfer path analysis method based on parametric load models. *Mechanical Systems and Signal Processing* 25: 1321–1338.
- Jiang H, Wu H, Yu L., et al. (2019) Force identification based on the reconstruction of distributed response with an optimized sensor placement. *Proceedings of the Institution of Mechanical Engineers, Part C: Journal of Mechanical Engineering Science* 233(1): 108–119.
- Lage YE, Maia NM., Neves MM, et al. (2013) Force identification using the concept of displacement transmissibility. *Journal of Sound and Vibration* 332(7): 1674–1686.
- Leclère Q and Pézerat C (2012) Vibration source identification using corrected finite difference schemes. *Journal of Sound and Vibration* 331: 1366–1377.
- Lee HP, Lim SP and Khun MS (2006) Diversion of energy flow near crack tips of a vibrating plate using the structural intensity technique. *Journal of Sound and Vibration* 296: 602–622.
- Li K, Liu J, Han X, et al. (2015) A novel approach for distributed dynamic load reconstruction by space-time domain decoupling. *Journal of Sound and Vibration* 348: 137–148.
- Liu Y and Shepard WS, Jr (2006) An improved method for the reconstruction of a distributed force acting on a vibrating structure. *Journal of Sound and Vibration* 291: 369–387.
- Liu Y and Shepard WS, Jr (2005) Dynamic force identification based on enhanced least squares and total least-squares schemes in the frequency domain. *Journal of Sound and Vibration* 282: 37–60.
- Ma C-K, Chang J-M and Lin D-C (2003) Input forces estimation of beam structures by an inverse method. *Journal of Sound and Vibration* 259(2): 387–407.
- Meirovitch L (2001) *Fundamentals of Vibrations*. Boston: McGraw-Hill.
- Pezerat C and Guyader JL (2000a) Identification of vibration sources. *Applied Acoustics* 61: 309–324.2000
- Pezerat C and Guyader JL (2000b) Force analysis technique: reconstruction of force distribution on plates. *Acustica United with Acta Acustica* 86: 322–332.
- Qiao B, Chen X, Luo X, et al. (2015) A novel method for force identification based on the discrete cosine transform. *Journal of Vibration and Acoustics* 137: 051012.
- Qiao B, Zhang X, Wang C, et al. (2016) Sparse regularization for force identification using dictionaries. *Journal of Sound and Vibration* 368: 71–86.
- Samet A, Ben Souf MA, Bareille O, et al. (2017) Vibration sources identification in coupled thin plates through an inverse energy method. *Applied Acoustics*: 12883–12893.
- Thite AN and Thompson DJ (2003) The quantification of structure-borne transmission paths by inverse methods. part 1: improved singular value rejection methods. *Journal of Sound and Vibration* 264(2): 411–431.
- Tse FS, Morse I and Hinkle RT (1978) *Mechanical Vibrations: Theory and Applications*. Hoboken, NJ: Prentice-Hall.
- Wang CQ, Ong EH, Qian H, et al. (2006) On the application of B-spline approximation in structural intensity measurement. *Journal of Sound and Vibration* 290: 508–518.
- Wang XQ, Wong WO and Cheng L (2009) Modal power flow with application to damage detection. *International Journal of Engineering Science* 47: 512–523.
- Wong WO, Wang XQ and Cheng L (2009) Modal power flow analysis of a damaged plate. *Journal of Sound and Vibration* 320: 84–100.
- Xu H, Cheng L, Su Z, et al. (2011) Identification of structural damage based on locally perturbed dynamic equilibrium with an application to beam component. *Journal of Sound and Vibration* 330: 5963–5981.

Appendix A

Effect of boundary conditions on the modal energy density of a beam

Modal energy density of the beam at the location of the exciting force may be written as

$$\Gamma_{jk} E_{jk}(x_f) = \frac{F^2}{4(\omega_j^2 - \omega_f^2)(\omega_k^2 - \omega_f^2)} \times \left[m(x)\omega_f^2 W_j(x_f)^2 W_k(x_f)^2 + YI(x) W_j(x_f) W_k(x_f) \times \frac{d^2(W_j(x_f))}{dx^2} \frac{d^2(W_k(x_f))}{dx^2} \right], j \neq k \quad (23)$$

where $W_j(x)$ and $W_k(x)$ are the j^{th} and k^{th} mode shapes of the beam, respectively. If just high-order modes where $\omega_i > \omega_f$, $\omega_r > \omega_f$ are considered, then the sign of $\Gamma_{jk} E_{jk}(x_f)$ depends only on the sign of $W_r(x_f) d^2(W_r(x_f))/dx^2$.

Table A1. Boundary conditions and coefficient relationship.

Boundary condition	Mathematics description	Coefficient relationship
Pin end	$w _{x=0} = 0$	$B + D = 0$
	$\frac{\partial^2 w}{\partial x^2} \Big _{x=0} = 0$	$-B + D = 0$
Fix end	$w _{x=0} = 0$	$B + D = 0$
	$\frac{\partial w}{\partial x} \Big _{x=0} = 0$	$A + C = 0$
Free end	$\frac{\partial^2 w}{\partial x^2} \Big _{x=0} = 0$	$-B + D = 0$
	$\frac{\partial^3 w}{\partial x^3} \Big _{x=0} = 0$	$-A + C = 0$

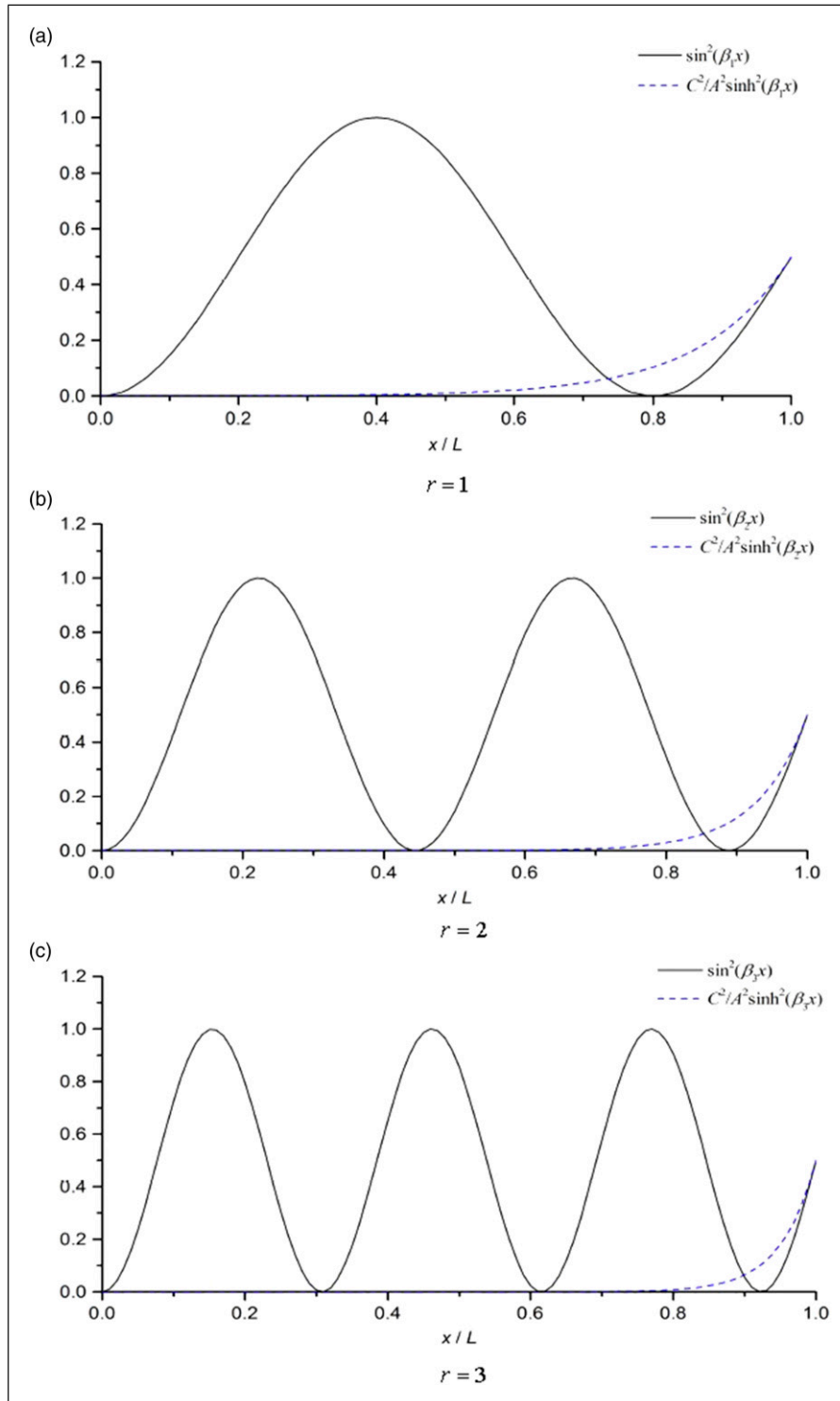


Fig. A1 Effect of pinned-free/fixed boundary conditions on the FLI.

Since the exciting force can be applied anywhere along the beam, the symbol x_f is substituted by x , which does not affect the result in the following analysis. To analyze the sign of $W_r(x)$ $d^2(W_r(x))/dx^2$, results are enumerated under

all the combinations of the classical boundary conditions including pinned, fixed, and free end of the beam.

The mode shape of an Euler–Bernoulli beam may be written as

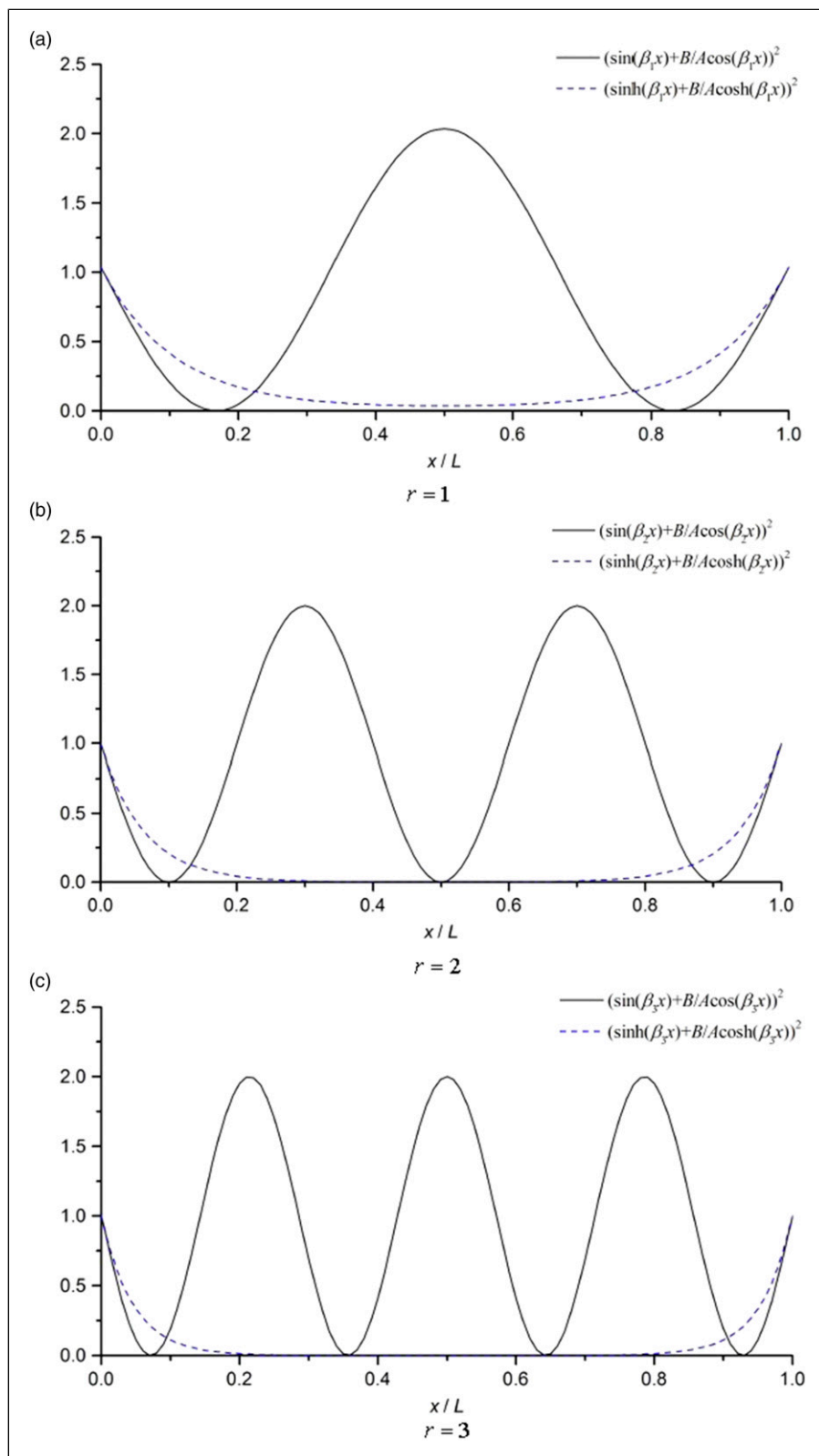


Fig. A2 Effect of free/fixed-free/fixed boundary conditions on the FLI.

$$W_r(x) = A \sin(\beta_r x) + B \cos(\beta_r x) + C \sinh(\beta_r x) + D \cosh(\beta_r x) \quad (24)$$

where A , B , C , and D are constants to be determined by the boundary conditions, and β_r is

$$\beta_r^4 = \frac{\omega_r^2 m}{YI} \quad (25)$$

By using the general form of mode shape, we may write

$$W_r(x) \frac{d^2(W_r(x))}{dx^2} = -\beta_r^2 ((A \sin(\beta_r x) + B \cos(\beta_r x))^2 - (C \sinh(\beta_r x) + D \cosh(\beta_r x))^2) \quad (26)$$

Some of the relationships among the coefficients in equation (26) may be determined by the boundary conditions at the location $x = 0$, as shown in Table A1.

In general, there are two sets of boundary conditions that need to be considered: pinned end and fixed or free (fixed/free) end for the sign of $W_r(x) d^2(W_r(x))/dx^2$. Three different combinations of the boundary conditions of the beam are considered in the following.

(a) Pinned–pinned boundary conditions

For a pinned end at $x = 0$, $B = D = 0$. Equation (26) is simplified as

$$W_r(x) \frac{d^2(W_r(x))}{dx^2} = -\beta_r^2 A^2 \left(\sin^2(\beta_r x) - \frac{C^2}{A^2} \sinh^2(\beta_r x) \right) \quad (27)$$

For the pinned–pinned boundary conditions, the pinned end at $x = L$ results in $C = 0$. Therefore, the sign of $W_r(x) d^2(W_r(x))/dx^2$ is determined by $-\sin^2(\beta_r x)$ in equation (27), which is always negative. Therefore, $\Gamma_{jk} E_{jk}(x_f)$ of equation (23) is positive throughout the beam span if $\omega_i > \omega_f$, $\omega_r > \omega_f$.

(b) Pinned-free and pinned-fixed boundary conditions

For pinned-free/fixed boundary condition, the component $\sinh^2(\beta_r x)$ also has effect on the sign. The free/fixed end condition results in the coefficient relationship

$$\frac{C^2}{A^2} = \frac{\sin^2(\beta_r L)}{\sinh^2(\beta_r L)} \quad (28)$$

The effects of $\sin^2(\beta_r x)$ and $C^2/A^2 \sinh^2(\beta_r x)$ in equation (27) are calculated and plotted in Figure A1 to show their effects on the accumulation phenomenon of the FLI along the beam. It could be seen in Figure A1 that with the increase of the order of mode r , the effect of hyperbolic component $\sinh^2(\beta_r x)$ is gradually shifted to the free/fixed end. Therefore, when considering high-order modes, the effects of the boundary conditions to the FLI can be neglected if x satisfy the condition (29) below

$$\sin^2(\beta_r x) > \frac{\sin^2(\beta_r L)}{\sinh^2(\beta_r L)} \sinh^2(\beta_r x) \quad (29)$$

(c) Free/fixed-free/fixed boundary conditions

For the free/fixed end at $x = 0$, we have $B = -D$ $A = -C$ or $B = D$ $A = C$ Equation (26) may be simplified as

$$W_r(x) \frac{d^2(W_r(x))}{dx^2} = -\beta_r^2 A^2 \left(\left(\sin(\beta_r x) + \frac{B}{A} \cos(\beta_r x) \right)^2 - \left(\sinh(\beta_r x) + \frac{B}{A} \cosh(\beta_r x) \right)^2 \right) \quad (30)$$

For free/fixed-free/fixed boundary condition, the hyperbolic component $(\sinh(\beta_r x) + B/A \cosh(\beta_r x))^2$ also has effect on the sign of $W_r(x) d^2(W_r(x))/dx^2$. The free/fixed end condition results in the coefficient relationship

$$\frac{B}{A} = \frac{\sin(\beta_r L) \sinh(\beta_r L)}{\cos(\beta_r L) - \cosh(\beta_r L)} \quad (31)$$

The effects of both the components in equation (29) on the accumulation phenomenon along the beam are shown in Figure A2, when the order of mode r is increasing. Similar to the results in pinned-free/fixed boundary conditions, the effects of the hyperbolic components caused by fixed/free end condition just affect the region near the boundary. With the increase of mode order, that region becomes smaller and closer to the boundary. This shows that if we consider only the high-order modes of the beams, the sign of $W_r(x) d^2(W_r(x))/dx^2$ is negative if x satisfy the condition (32) below

$$\left(\sin(\beta_r x) + \frac{\sin(\beta_r L) \sinh(\beta_r L)}{\cos(\beta_r L) - \cosh(\beta_r L)} \cos(\beta_r x) \right)^2 > \left(\sinh(\beta_r x) + \frac{\sin(\beta_r L) - \sinh(\beta_r L)}{\cos(\beta_r L) - \cosh(\beta_r L)} \cosh(\beta_r x) \right)^2 \quad (32)$$

To sum up, according to the results shown with either fixed, free, or pinned boundary condition, the proposed force localization index (FLI) can be applied to the whole beam span for beams with pinned–pinned boundary conditions. The FLI can be applied to beams with pin-free or pin-fixed boundary conditions at location x satisfying condition (29). The FLI can be applied to beams with free/fixed-free/fixed boundary conditions at location x satisfying condition (32).

Appendix B

FLI of a step beam structure

The eigenvalue solution of a step beam derived below follows the approach of Wong et al. (2009). Consider a step beam with different stiffness at different sections as

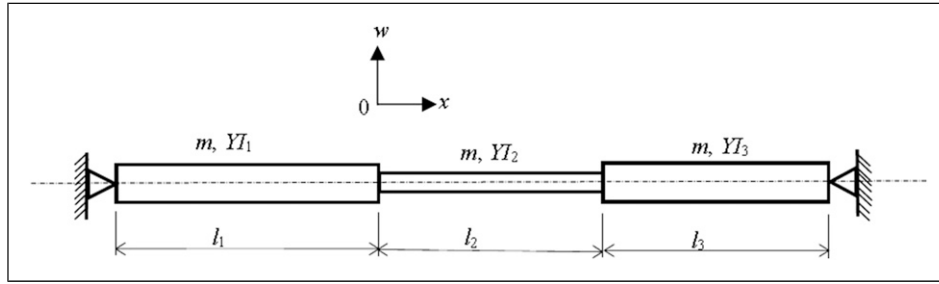


Fig. B1 Step beam with pinned-pinned boundary conditions.

illustrated in Figure B1. Applying Euler–Bernoulli beam theory to the step beam, the governing differential equation of each section of the beam can be expressed as

$$\begin{aligned}
 YI_1 \frac{\partial^4 w_1}{\partial x^4} + m \frac{\partial^2 w_1}{\partial t^2} &= 0 & -l_1 < x < 0 \\
 YI_2 \frac{\partial^4 w_2}{\partial x^4} + m \frac{\partial^2 w_2}{\partial t^2} &= 0 & 0 < x < l_2 \\
 YI_3 \frac{\partial^4 w_3}{\partial x^4} + m \frac{\partial^2 w_3}{\partial t^2} &= 0 & l_2 < x < l_3
 \end{aligned} \tag{33}$$

where m is the mass per length of the beam, and w_1 , w_2 , and w_3 are the transverse vibratory displacements of the Sections 1-3 of the beam, respectively.

The general solutions of equation (33) are

$$\begin{aligned}
 w_i(x, t) &= (A_i \sin \beta_i x + B_i \cos \beta_i x + C_i \sinh \beta_i x \\
 &\quad + D_i \cosh \beta_i x) e^{i\omega t}, \quad i = 1, 2, 3
 \end{aligned} \tag{34}$$

where j is the imaginary number $\sqrt{-1}$; $\beta_i = (m\omega^2/YI_i)^{1/4}$ and i is the number to identify the spans shown in Figure B1.

The mode shape function of the beam is the spatial part of equation (34) written as

$$\begin{aligned}
 w_i(x, t) &= (A_i \sin \beta_i x + B_i \cos \beta_i x \\
 &\quad + C_i \sinh \beta_i x + D_i \cosh \beta_i x), \quad i = 1, 2, 3
 \end{aligned} \tag{35}$$

To satisfy the continuity and equilibrium conditions at the junctions of the sections, the following set of equations is derived

$$\begin{aligned}
 w_1(0, t) &= w_2(0, t), w'_1(0, t) = w'_2(0, t), \\
 YI_1 w''_1(0, t) &= YI_2 w''_2(0, t), YI_1 w'''_1(0, t) = YI_2 w'''_2(0, t), \\
 w_2(l_2, t) &= w_3(l_2, t), w'_2(l_2, t) = w'_3(l_2, t), \\
 YI_2 w''_2(l_2, t) &= YI_3 w''_3(l_2, t), YI_2 w'''_2(l_2, t) = YI_3 w'''_3(l_2, t)
 \end{aligned} \tag{36}$$

where primes denote differentiation with respect to x .

The boundary conditions of the step beam can be expressed as

$$[K_1] \begin{bmatrix} A_1 \\ B_1 \\ C_1 \\ D_1 \end{bmatrix} + [K_3] \begin{bmatrix} A_3 \\ B_3 \\ C_3 \\ D_3 \end{bmatrix} = \begin{bmatrix} 0 \\ 0 \\ 0 \\ 0 \end{bmatrix} \tag{37}$$

where $[K_1]$ and $[K_3]$ depend on the actual arrangements of the boundary conditions of the beam. At the first junction at origin O , the continuity and equilibrium conditions combined with equation (36) lead to a simple relationship between coefficients for Section 1 and Section 2. Such relationship can be written as

$$\begin{bmatrix} A_1 \\ B_1 \\ C_1 \\ D_1 \end{bmatrix} = [A_1] \begin{bmatrix} A_2 \\ B_2 \\ C_2 \\ D_2 \end{bmatrix} \tag{38}$$

where

$$[A_1] = \frac{1}{2} \begin{bmatrix} \beta_2/\beta_1 + \beta_1/\beta_2 & 0 & \beta_2/\beta_1 - \beta_1/\beta_2 & 0 \\ 0 & 1 + \beta_1^2/\beta_2^2 & 0 & 1 - \beta_1^2/\beta_2^2 \\ \beta_2/\beta_1 - \beta_1/\beta_2 & 0 & \beta_2/\beta_1 + \beta_1/\beta_2 & 0 \\ 0 & 1 - \beta_1^2/\beta_2^2 & 0 & 1 + \beta_1^2/\beta_2^2 \end{bmatrix} \text{ is a ma-}$$

trix relating the coefficient vector $[A_1 \ B_1 \ C_1 \ D_1]^T$ of Section 1 and the coefficient vector $[A_2 \ B_2 \ C_2 \ D_2]^T$ of Section 2.

For the junction of Sections 2 and 3, we can translate the origin of the coordinates to the junction. By carrying out the coordinate transformation on equation (38), we have

$$[T_L] \begin{bmatrix} A_2 \\ B_2 \\ C_2 \\ D_2 \end{bmatrix} = [A_2] [T_R] \begin{bmatrix} A_3 \\ B_3 \\ C_3 \\ D_3 \end{bmatrix} \tag{39}$$

where

$$[A_2] = \frac{1}{2} \begin{bmatrix} \beta_3/\beta_2 + \beta_2/\beta_3 & 0 & \beta_3/\beta_2 - \beta_2/\beta_3 & 0 \\ 0 & 1 + \beta_2^2/\beta_3^2 & 0 & 1 - \beta_2^2/\beta_3^2 \\ \beta_3/\beta_2 - \beta_2/\beta_3 & 0 & \beta_3/\beta_2 + \beta_2/\beta_3 & 0 \\ 0 & 1 - \beta_2^2/\beta_3^2 & 0 & 1 + \beta_2^2/\beta_3^2 \end{bmatrix} [T_L] \text{ and}$$

$[T_R]$ are two coordinate transfer matrices and written as

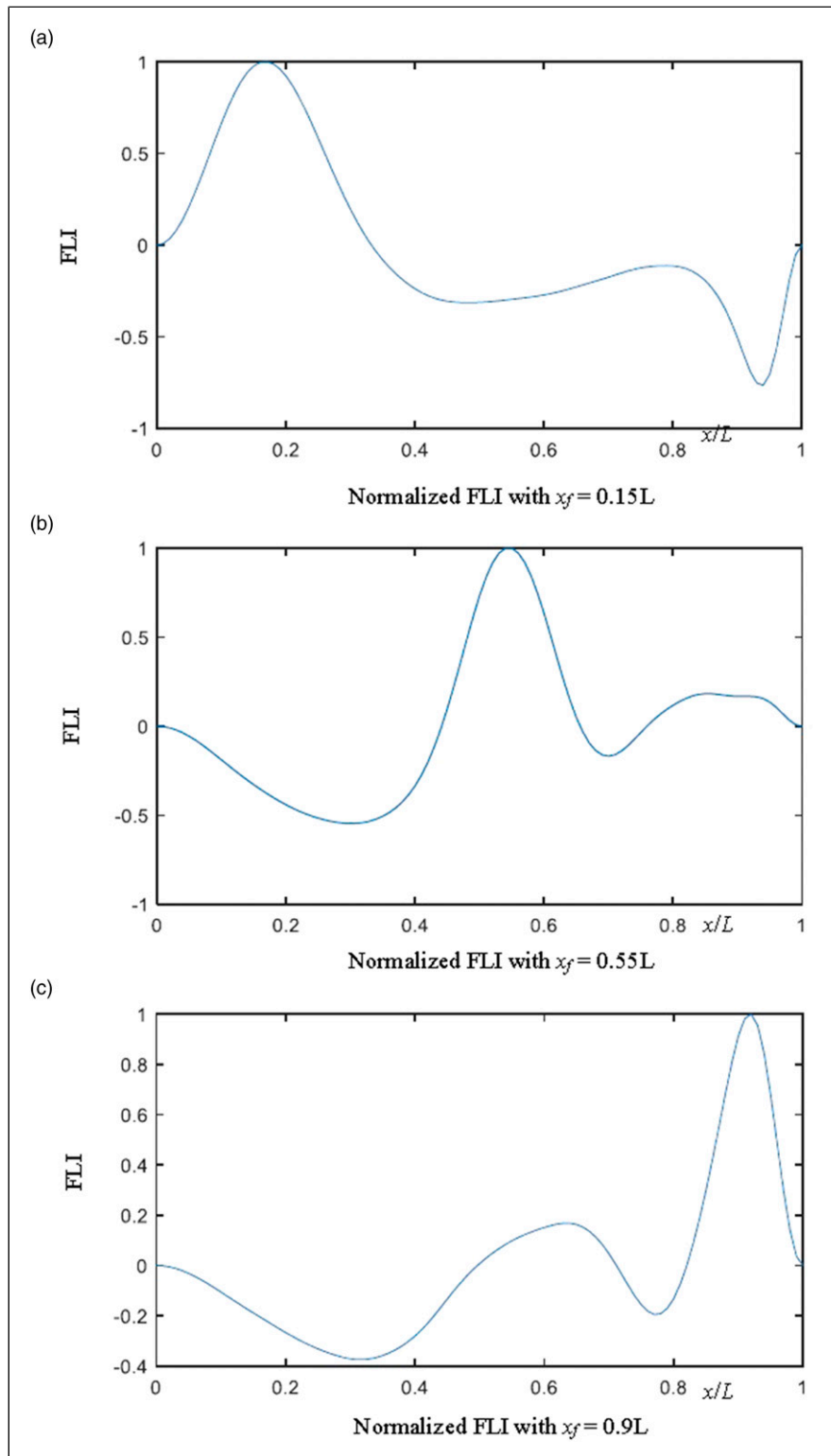


Fig. B2 Step beam with pinned-pinned boundary conditions.

$$[T_L] = \begin{bmatrix} \cos \beta_2 l_2 & -\sin \beta_2 l_2 & 0 & 0 \\ \sin \beta_2 l_2 & \cos \beta_2 l_2 & 0 & 0 \\ 0 & 0 & \cosh \beta_2 l_2 & \sinh \beta_2 l_2 \\ 0 & 0 & \sinh \beta_2 l_2 & \cosh \beta_2 l_2 \end{bmatrix} \quad (40)$$

$$[T_R] = \begin{bmatrix} \cos \beta_3 l_2 & -\sin \beta_3 l_2 & 0 & 0 \\ \sin \beta_3 l_2 & \cos \beta_3 l_2 & 0 & 0 \\ 0 & 0 & \cosh \beta_3 l_2 & \sinh \beta_3 l_2 \\ 0 & 0 & \sinh \beta_3 l_2 & \cosh \beta_3 l_2 \end{bmatrix} \quad (41)$$

Substitute equation (38) into equation (39), the relationship between the coefficients of Section 1 and those of Section 3 can be expressed as

$$\begin{bmatrix} A_1 \\ B_1 \\ C_1 \\ D_1 \end{bmatrix} = [A_1][T_L]^{-1}[A_2][T_R] \begin{bmatrix} A_3 \\ B_3 \\ C_3 \\ D_3 \end{bmatrix} \quad (42)$$

Substitute this equation into equation (37), the eigenvalue problem can be expressed as

$$\{[K_1][A_1][T_L]^{-1}[A_2][T_R] + [K_3]\} \begin{bmatrix} A_3 \\ B_3 \\ C_3 \\ D_3 \end{bmatrix} = \begin{bmatrix} 0 \\ 0 \\ 0 \\ 0 \end{bmatrix} \quad (43)$$

For a non-trivial solution, the determinant of the 4 x 4 matrix in equation (43) should be zero; that is

$$|[K_1][A_1][T_L]^{-1}[A_2][T_R] + [K_3]| = 0 \quad (44)$$

The eigenvalues ω^2 can be obtained by solving the eigenvalue problem represented by equation (44). Substituting these eigenvalues into equation (43) and solving it together with equation (37) and (39), the coefficient vector $[A_i \ B_i \ C_i \ D_i]^T$ for the corresponding beam spans can be obtained. Substituting the vector $[A_i \ B_i \ C_i \ D_i]^T$ into equation (35), the corresponding eigenfunctions (mode shapes), $w_i(x)$, are obtained. These mode shape functions are used for the calculation of FLI in equation (20) for the step beam.

A numerical experiment was done to test the proposed FLI for a step beam. A pinned–pinned step beam with three sections as illustrated in Figure B1 was used in the test. For illustration purpose, it was assumed that $YI_1 = YI_3 = 2YI_2 = 1$, $m = 1$, $l_1 = 0.4L$, and $l_2 = l_3 = 0.3L$. The eigenvalues ω^2 and the mode shape functions $w_i(x)$ of the step beam were calculated according to the theory as described above. The forcing frequency was assumed to be in between the first and the second natural frequencies of the step beam. The FLIs of the step beam were calculated using natural frequencies and mode shapes from the second to the seventh natural modes of the step beam according to equation (20) with $x/L = 0.15, 0.55, \text{ and } 0.9$, respectively. The FLI results were plotted in Figure B2. As shown in Figure B2, highest peak value of FLI could be observed at the exciting force location in all the three cases. The proposed FLI was found to be applicable to a step beam.